Characterization of electro-optical first order properties of lithium niobate slab

H. J. d'Nóbrega

13^{th} November 2017

Abstract

In this paper, the electro-optic properties of a lithium niobate slab were analyzed.

Qualitatively, we analyzed the general dependence of the phase shift between light beams from both arms of Michelson-Morley and Mach-Zender interferometers on the voltage that created an electric field inside the slab, and verified the dominance of the linear Pockels coefficients over the Kerr quadratic ones, with r^2 of over 0.9990, for two different polarizations of the light beam.

Quantitatively, we supposed three relative orientations of the natural optical axis of the sample and derived the error in assuming each one of them, considering the experimental data. No conclusion could be drawn from such data, given the error percentages that ranged from 27.68% to 89.58%.

1 Introduction

In recent times, there has been a progressive interest in the possibility of controling several optical properties of materials, namely through external applied fields. In the case such field is an electric field, we are presented with the electro-optic effect.

The manipulation of, for instance, the refractive index may be relevant in areas which range from photonics [1], to spectroscopy (and all its subsidiaries), signal processing and optical communications (production of intensity modulators and so forth).

Considering that the interaction of $\mathbf{E}$ fields with matter through the polarization $\mathbf{P}$ is well documented, and so is the nature of light as an electromagnetic wave, it suffices to assume that the permitivity tensor $\hat{\epsilon}$ is perturbed in the presence of external $\mathbf{E}$. Defining $\eta_{ij} = \frac{\epsilon_0}{\epsilon_{ij}}$, we have , up to second order in $\mathbf{E}$ [2]

$$\eta_\alpha = \eta_\alpha(0) + \sum_k r_{\alpha k} E_k + \sum_{k,l} s_{\alpha k l} E_k E_l, \qquad (1)$$

where the r factors are known as the Pockels coefficients and the s ones as the Kerr coefficients, usually of lesser numerical importance.

Considering a non-centrosymmetrical material, exhibiting natural birefringency characterized by the indices n_e and n_o, the external $\mathbf{E}$ field has the effect of altering these refractive indices. In the case of lithium niobate ($LiNbO_3$), the Pockels coefficients are arranged in the matrix

$$r_{ij}[\mathrm{pmV}^{-1}]^1 = \begin{bmatrix} 0 & -3.4 & 8.6 \\ 0 & 3.4 & 8.6 \\ 0 & 0 & 30.8 \\ 0 & 28 & 0 \\ 28 & 0 & 0 \\ -3.4 & 0 & 0. \end{bmatrix} \qquad (2)$$

To account for this effect, an interferometric device can be used, where one arm is kept as a reference and the other one contains a slab of a material exhibiting appreciable electro-optic effect. An interference pattern may be observed, produced by the phase shift between the light waves.

[1] Unless units are included near a physical quantity, the values presented are to be considered as the SI ones.

If the index of refraction of the slab of length L is varying with an applied electric field, elementary optics considerations yield

$$\Delta\phi = mL\frac{2\pi}{\lambda_0}P(E) \tag{3}$$

where m is a parameter concerning the interferometer – for instance, one for a Mach-Zender (MZ) and two for a Michelson-Morley (MM) – and P is a parameter concerning the refractive index "seen" by the light ray inside the sample, dependent of the intensity of the applied electric field E.

The intensity of the light beam captured by a detector varies with $\Delta\phi$, according to

$$I = I_{\substack{\text{ref.}\\ \text{beam}}} + I_{\substack{\text{slab}\\ \text{beam}}} + 2\sqrt{I_{\substack{\text{ref.}\\ \text{beam}}} I_{\substack{\text{slab}\\ \text{beam}}}}\sin(\Delta\phi). \tag{4}$$

Therefore, the variation of E produces a translation of the interference pattern by varying I.

Finally, the angle between the direction of the natural optical axis $\mathbf{e_o}$ of the sample and that of the applied $\mathbf{E}$ field affects the dependence of P in $|\mathbf{E}|$. Some directions of the incident polarization are of particular interest:

1. $\mathbf{E}$ paralell to $\mathbf{e_o}$: the principal axis remain unaltered and the new eigenindexes are

$$n^*_{o,e} = n_{o,e} - \frac{n^3_{o,e}}{2}r_{13,33}E. \tag{5}$$

If the polarization of the wave is paralell (perpendicular) to $\mathbf{e_o}$, we arrive at the simple expression $P = n^*_{o,e}(E)$, by taking the respective subscript.

2. $\mathbf{E}$, $\mathbf{e_o}$ and $\mathbf{k}$ mutually ortogonal, with $\mathbf{E}$ paralell to the $\mathbf{e_y}$ direction of the perturbed permitivity tensor: the crystal is now biaxial with

$$\begin{aligned} n_x &= n_o + \frac{n_o^3}{2}r_{22}E \\ n_y &= n_o - \frac{n_o^3}{2}r_{22}E + \frac{n_o^3 n_e^4}{n_o^2 - n_e^2}(r_{42}E)^2 \\ n_z &= n_e - \frac{1}{2}\frac{n_o^3 n_e^4}{n_o^2 - n_e^2}(r_{42}E)^2. \end{aligned} \tag{6}$$

The new principal axis are the $\mathbf{e_k}$ axis, and both the optical axis and the $\mathbf{e_E}$ axis rotated of $\theta << 1$ such that

$$\tan\theta \approx \sin\theta \approx \theta \approx -\frac{n_o^2 n_e^2 r_{42}E}{n_o^2 - n_e^2}. \tag{7}$$

If the beam is polarized paralelly (perpendicularly) to $\mathbf{e_o}$, we have, respectively,

$$P \approx n_{z,y} - \theta(n_y - n_z). \tag{8}$$

3. $\mathbf{E}$ perpendicular to $\mathbf{e_o}$ and the latter paralell to k and to the $\mathbf{e_y}$ direction of the perturbed permitivity tensor: the new eigenindices are given by 6 and $\mathbf{e_o}$ and $\mathbf{e_E}$ are rotated of θ from Eq.7.

Upon considering the propagation of the beam inside the crystal, one arrives at

$$P = \frac{n_e n_o}{(n_e^2 + n_o^2)^{1/2}}(1 + \frac{r_{22}}{2}\frac{n_e^2}{n_e^2 + n_o^2}E) \tag{9}$$

which is valid independently of the incident polarization, inasmuch as $\mathbf{e_k}$ is approximately paralell to an optical axis.

2 Experimental setup

Depending on the interferometric device, two experimental setups were used, which are schematically represented in Figs.1,2. The Mach-Zender apparatus was also photographed for further reference (Fig.3).

The light source is a HeNe laser operating at 632.8nm with maximum power output of 10mW. The slab's thickness $d = 1.00 \pm 0.01$mm and length, in the direction paralell to the beam's wavevector, $L = 4.74 \pm 0.05$cm were recorded for future calculations.

If the interferometers are propperly alligned, it is expected for the laser beam to be splited equally in the first beam splitter and follow identical physical paths along both arms of the interferometer. The two beams are recombined in the second beam splitter and interferometric phenomena may be observed

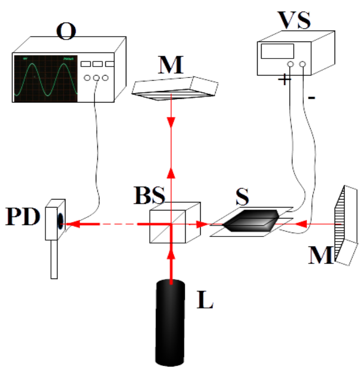

Figure 1: Diagram of the experimental setup with a MM interferometer, featuring the laser source (L), the two beam spliters (BS), the voltage source (VS), oscilloscope (O), photodetector (PD), lens (L), mirrors (M) and the $LiNbO_3$ slab (S).

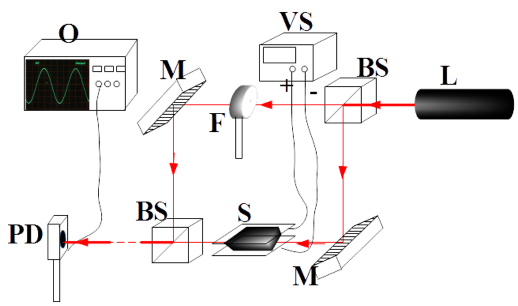

Figure 2: Diagram of the experimental setup with a MZ interferometer, with the same labels of Fig.1 and a neutral density filter for optical power balance between the two arms (F).

as far away as the photodetector PDA100A-EC by Thor Labs is placed. The photodetector was then connected to the oscilloscope Textronic 1001C-EDU.

3 Experimental method

Considering the nature of the experiment, several precautions were necessary.

Concerning the Michelson-Morley (MM) interferometer, the allignment was performed in the follwing manner: firstly, the beam splitter was placed, after which the mirrors were placed, and their desired directions were checked. Finally, we placed all other components, such as the polarizer and analyzer and the photodetector in the path of the respective rays.

The Mach-Zender (MZ) interferometer was more difficult to allign correctly. Firstly, the laser and first beam splitter were placed and kept horizontal. Secondly, verifications were made concerning the horizontality of the reference beam's plane and the 45 degree angle the mirrors should be placed at. Finally, the branch with the sample was set and the final alignment of the second beam splitter was performed. The observation of interference fringes (Fig.4) allowed us to confirm that the interferometer was duely assembled.

An approximate balance of optical power amongst both arms of the interferometer was attained by using a beam intensity filter in reference arm.

The introduction of the thin film in both interferometers was carried out at last, bearing in mind the following features:

- the light beam was parcially reflected in the thin film's transversal face, and those reflections had to be controled and redirected to avoid the path of important light beams;
- possibly due to irregularities in the cut of the thin film, the alignment of the Mach-Zender was perturbed by such introduction, which required a re-allignment;
- the thin film had to be tilted on both the longitudinal and transversal axes, so as to minimize the occurence of a second light beam emergence, and focus the relevant light beam.

4 Experimental observations and results

For future reference, the reader may find the theoretical predictions for each of the numbered cases present in Sec.1 in terms of the expected curve $V_{PD} = V_0 + A\sin(\omega V_{app} + \phi_0)$, using the refractive indices for

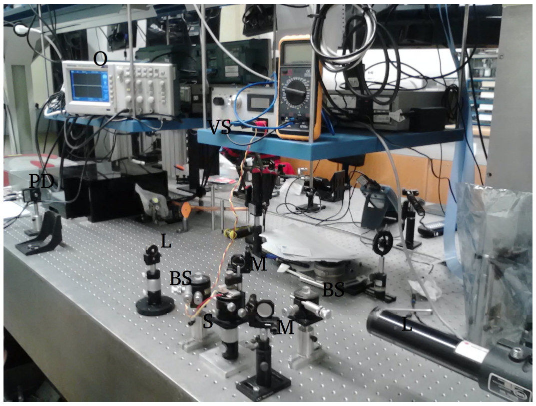

Figure 3: Experimental setup for the analysis of the electro-optic effect using a MZ interferometer, with the same labels of Figs.1 and 2.

Case number	Pol.	1	2	3
ω	PP	2.398	7.443	1.288
	NP	0.955	6.488	1.288
ϕ_0	PP	1.223	1.223	1.5862
	NP	0.254	0.2545	1.5862

Table 1: Theoretical fitting parameters for each of the cases presented in 1 and considering a MZ apparatus. The ω values are to be multiplied by 10^{-2}. For a MM interferometer, the theoretical values should be the double of the above.

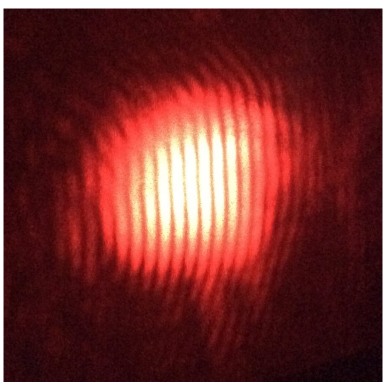

Figure 4: Observed interferometric phenomena using the MZ interferometer.

$LiNbO_3$ at 632.8nm [5]. A quick analysis allows us to understand that we are dealing with an effect of very subtle magnitude and that high exactness is required to assure that the results are a good indicator of the sample's orientation.

Those levels of exactness may not be achievable through this experimental setup, for reasons concerning the uncertainty in the horizontal placement of the slab and the perfect allignment of the interferometers, for instance.

Finally, considerations regarding the extreme sensitivity of the experiment to external perturbations were taken into account by performing it in a closed room, with all light sources but the laser off and the computer where the data was recorded also away from the setup. Both experiments were carried out over a Melles Griot optical table.

The relation between the applied voltage and the applied field is given by $V_{app} = \frac{E}{d}$.

The conversion between the voltage read in the osciloscope may be computed from the datasheet of the PD, considering we used a gain of 4 dB in the PD: $I \approx 3.3 \times 10^{-13} V_{PD}$. This conversion affects only the amplitude of the sinusoidal dependence showed in 4; therefore, it was chosen to work with the actual voltage signal from the PD.

4.1 Michelson-Morley interferometer

For each applied voltage, the voltage measured in the PD was recorded. The variation of the applied voltage was performed manually. We waited for the signal in the oscilloscope to stabilize around a central value before recording the PD voltage. The data obtained with the Michelson-Morley experiment are shown in Fig.5.

The ω value thus obtained is far from all expected values by one order of magnitude. The sinusoidal trend was confirmed, therefore it is evident that methodologic errors may have occured. In fact, the slab might not be perfectly alligned with the beam, and reflections may have occured inside it, with a double emphasis because light travels twice given the interferometer's configuration.

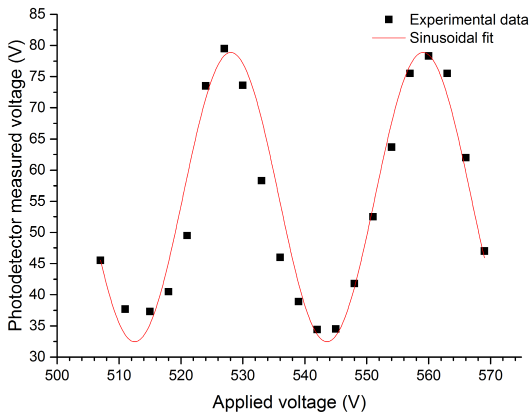

Figure 5: Voltage measured by the PD using the Michelson-Morley interferometer for several values of applied voltage.

Parameter	PP
A	23.2121 ± 0.8473
ω	0.2024 ± 0.0031
ϕ_0	0.7609 ± 0.2801
I_0	55.6686 ± 0.7271
r^2	0.99995

Table 2: Fit parameters for the MM apparatus and incident beam polarization paralell to the table (PP).

Additionally, no recording of the electro-optic effect using a perpenducular polarization of the laser was used.

This showed the need to use a different interferometric device, leading to a new experiment conducted weeks later.

4.2 Mach-Zender interferometer

The procedure was analogous to the MM interferometer, but now a maximum and minimum value for the PD voltage was recorded. This allowed to consider V_{PD} the average of these values and assign to it its uncertainty σ^2 given as the standard deviation of those same values.

Parameter	PP	NP
A	1.099 ± 0.043	1.6369 ± 0.1249
ω	0.0455 ± 0.0006	0.0177 ± 0.0004
ϕ_0	0.7784 ± 0.1052	-1.4429 ± 0.3264
I_0	1.3552 ± 0.0338	2.2036 ± 0.0931
r^2	0.99995	0.99994

Table 3: Fit parameters for the Mach-Zender apparatus and incident beam polarizations paralell and perpendicular to the plane of the table (PP and NP, respectively).

Case number	1	2	3
PP	89.58	38.84	71.86
NP	84.37	72.72	27.68

Table 4: Exactness percentages for ω considering each of the numbered cases in Sec.1.

A sinusoidal weighted fit was performed using the program Origin 9.1. The weighting of the points – inversely proportional to their σ^2 – strongly improved the correlation parameter r^2. The sinusoidal trend of the data was verified and the fit parameters may be read from Tab. 3.

It is possible to observe that the obtained values for the period of the sinusoid, inversely proportional to ω, are different, which expresses the alteration of the index ellipsoid with the applied electric field.

There is no perfect match between data from both measured laser polarizations and the considered relative orientations of the optical axis, or even a slight error percentage. This seems to indicate that there is no special orientation of the cut of the crystal.

5 Conclusions and future work

In this work, the Pockels electro-optic effect was observed by means of light inteference both in Michelson-Morley (MM) and in Mach-Zender (MZ) apparatus using the same $LiNbO_3$ thin film. The unknown natural optical axis of the sample introduced an additional degree of freedom in the experiment, which was treated assuming specific cuts of the sam-

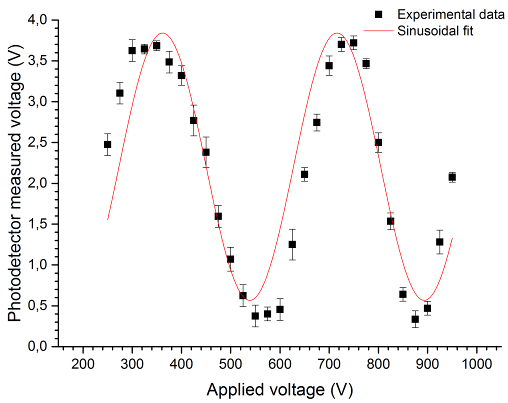

Figure 6: Voltage measured by the PD for several values of applied voltage and polarization paralell to the table using a MZ apparatus.

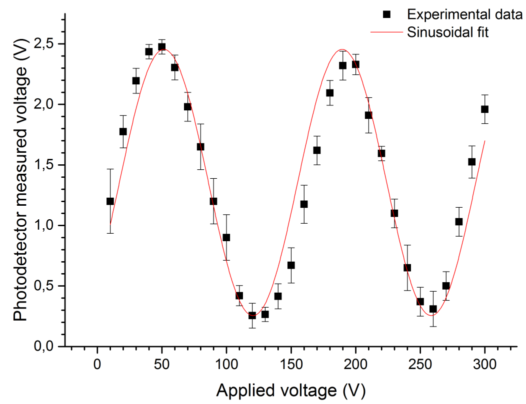

Figure 7: Voltage measured by the PD for several values of applied voltage and polarization perpendicular to the table using a MZ apparatus.

ple and computing the expected results for each of those three cases.

The assembly and propper allignment of two important optical system were also of great relevance to the unfamiliarized work group.

The MM apparatus yielded a result far from the expected results for specific orientations of the unknown natural optical axis of the sample by one order of magnitude, which may be explained by reflections inside the slab. However, it allowed us to conclude, with $r^2 = 0.9995$, that there is a sinusoidal variation of the interferometric intensity with the applied field – as was expected, the Pockels coefficients were dominant over the Kerr ones.

Finally, regarding the MZ apparatus, we obtained errors that ranged from 27.68% to 89.58%, which showed to be inconclusive in order to determine the orientation of the natural optical axis of the sample (also because the theoretical predictions are within the same order of magnitude and require exceptional exactness). The effects of reflections were minimized with this apparatus, lowering the obtained values for the frequency of the sinusoidal regression obtained with the MM interferometer to their expected order of magnitude. The correlation was yet again confirmed, showing the qualitative presence of an electro-optic effect of first order, with $r^2_{PP} = 0.99995$ and $r^2_{NP} = 0.99994$, for paralell and normal polarizations of the laser beam (relatively to the optical table).

It was concluded that this measurement was particularly sensitive to external noise, such as electric currents in the periphery and sound or movement. Ideal conditions were difficult to obtain and two data series were disregarded in account of this. As future work, a lock-in amplifier may be employed in order to further improve the signal-to-noise ratio and obtain more accurate results.

References

[1] M. Qasymeh, M. Cada, S. A. Ponomarenko. *Quadratic Electro-Optic Kerr Effect: Applications to Photonic Devices* IEEE Journal of Quantum Electronics, Vol.44, No.8, August 2008, pp. 740-746.

[2] J. A. Moreira. *Livro de apoio à disciplina de Materiais e Dispositivos Ópticos, chapter 7 - efeito eletro-ótico*

[3] M. Monteiro, M. Fernandes, Z. Coelho. *Estudo de alguns efeitos ópticos.* Essay for discipline Projecto Educacional, Sept. 2002.

[4] M. Born, E. Wolf. *Principles of Optics: Electromagnetic Theory of Propagation, Interference and Diffraction of Light*

[5] M. N. Polyanskiy. *Refractive index database* at `https://refractiveindex.info` Accessed on 2017-11-11